UC Berkeley
UC Berkeley Previously Published Works

Title

Self-organizing actin networks drive sequential endocytic protein recruitment and vesicle release on synthetic lipid bilayers

Permalink

Journal

Authors

Stoops, Emily H
Ferrin, Michael A
Jorgens, Danielle M
et al.

Publication Date

DOI

Copyright Information

Peer reviewed

Self-organizing actin networks drive sequential endocytic protein recruitment and vesicle release on synthetic lipid bilayers

Emily H. Stoops[a,1], Michael A. Ferrin[a,1], Danielle M. Jorgens[b], and David G. Drubin[a,2]

Forces generated by actin assembly assist membrane invagination during clathrin-mediated endocytosis (CME). The sequential recruitment of core endocytic proteins and regulatory proteins, and assembly of the actin network, are well documented in live cells and are highly conserved from yeasts to humans. However, understanding of CME protein self-organization, as well as the biochemical and mechanical principles that underlie actin's role in CME, is lacking. Here, we show that supported lipid bilayers coated with purified yeast Wiskott Aldrich Syndrome Protein (WASP), an endocytic actin assembly regulator, and incubated in cytoplasmic yeast extracts, recruit downstream endocytic proteins and assemble actin networks. Time-lapse imaging of WASP-coated bilayers revealed sequential recruitment of proteins from different endocytic modules, faithfully replicating in vivo behavior. Reconstituted actin networks assemble in a WASP-dependent manner and deform lipid bilayers, as seen by electron microscopy. Time-lapse imaging revealed that vesicles are released from the lipid bilayers with a burst of actin assembly. Actin networks pushing on membranes have previously been reconstituted; here, we have reconstituted a biologically important variation of these actin networks that self-organize on bilayers and produce pulling forces sufficient to bud off membrane vesicles. We propose that actin-driven vesicle generation may represent an ancient evolutionary precursor to diverse vesicle forming processes adapted for a wide array of cellular environments and applications.

actin | endocytosis | reconstitution | traffic | cell biology

Significance

Actin filament assembly participates in many vesicle-forming processes. However, the underlying principles for how assembly is initiated and organized to effectively harness assembly forces remain elusive. To address this gap, we report the reconstitution of actin-driven vesicle release from supported lipid bilayers. Using real-time imaging, we observe sequential recruitment of endocytic proteins and, following a burst of actin assembly, vesicle release from bilayers. Given the absence of cargo or upstream endocytic regulatory proteins on the bilayers, and the participation of actin in many vesicle-forming processes, we posit that this mode of vesicle formation represents an early evolutionary precursor for multiple trafficking pathways. We expect that this assay will be of great use for future investigations of actin-mediated vesicle-forming processes.

Clathrin-mediated endocytosis (CME) involves the recruitment of dozens of endocytic proteins to the plasma membrane where they collect cargo, deform the membrane, and drive vesicle scission. Endocytic protein recruitment follows a precise order and timing (1, 2), and can be roughly subdivided into a variable early phase during which clathrin and adapter components arrive at the membrane, and a highly regular late phase during which Wiskott Aldrich Syndrome Protein (WASP) and actin-associated proteins act at the endocytic site (3). Recruitment of *Saccharomyces cerevisiae* WASP (Las17, referred to hereafter as scWASP) to a threshold level promotes a burst of actin assembly through activation of the Arp2/3 complex, which nucleates actin polymerization (4). scWASP-mediated actin assembly is required to overcome the high turgor pressure of the yeast cell and drive membrane invagination (5).

With over 60 proteins involved in yeast endocytosis, many with nonessential roles or additional nonendocytic cellular functions, determining the functions of each protein in vivo has been challenging (6, 7). CME robustness often thwarts attempts at function elucidation; simultaneous deletion of seven genes encoding early endocytic proteins was shown to only minimally impact endocytosis (8). In vivo studies are well suited to identify necessary components of the CME machinery, but to identify components that are sufficient for CME and to gain insights into their biochemical mechanisms, we sought to reconstitute endocytic events in vitro. Biochemical reconstitution of cellular processes provides otherwise unattainable insight into fundamental molecular mechanisms (9). Reconstitution assays have been irreplaceable to test models and reveal mechanistic details for processes from pathogen motility in infected host cells (10–12) to mitotic spindle formation (13, 14). Of relevance to the work reported here, many important advances in our understanding of vesicle fusion and fission have come through in vitro reconstitutions (15–18). A reconstituted system for actin-mediated CME promises to reveal principles for properly ordered recruitment of CME proteins and the mechanics of membrane vesicle formation.

Here, we developed an in vitro assay that faithfully replicates the cooperative assembly of endocytic proteins onto synthetic membranes and deformation of the membrane into a nascent vesicle, resulting in actin-driven vesicle formation and release. We demonstrate

[1]E.H.S. and M.A.F. contributed equally to this work.

[2]To whom correspondence may be addressed. Email: drubin@berkeley.edu.

that scWASP-templated actin and endocytic protein network assembly alone are sufficient to direct membrane deformation and vesiculation from lipid bilayers. We suggest that WASP-mediated actin network assembly represents a minimal system to drive membrane invagination and vesicle scission and may represent an early evolutionary precursor for a wide variety of membrane trafficking modalities.

Results and Discussion

An in vitro actin assembly assay using polystyrene microbeads functionalized with scWASP was developed previously (19). When incubated in yeast cell extract, scWASP-coated beads assembled actin and selectively recruited endocytic actin network proteins. A fraction of the beads became motile. While this earlier reconstitution study represented an important advance for understanding the cooperative assembly of actin and actin-binding proteins involved in endocytosis, it did not allow conclusions to be drawn about the effect of the membrane on assembly of the actin network, or of actin network assembly on the membrane. To examine the effects of endocytic protein assembly on membranes we modified this system to include lipid bilayers (Fig. 1A). To that end, supported lipid bilayers were made on solid microspheres using established protocols that retain bilayer fluidity (*SI Appendix*, Fig. S1A).

Cytoplasmic extracts were prepared from yeast strains expressing at endogenous levels endocytic proteins tagged with fluorescent proteins (*SI Appendix, Table S1*). Since actin network nucleation on supported lipid bilayers was not observed in the absence of purified scWASP, this protein was purified and applied to the bilayers (Fig. 1 *B–D*). scWASP is one of the first actin regulators recruited to the endocytic site. Relative to proteins recruited to endocytic sites early in CME, scWASP arrival represents a more temporally regular progression from actin assembly to vesicle scission and internalization, thus making it a logical choice for this assay. Purified scWASP, previously shown to activate the Arp2/3 complex in vitro (20, 21), was efficiently recruited to supported lipid bilayers (Fig. 1 *C*). Although we engineered in a His-tag to bind scWASP to the Ni NTA supported lipid bilayers, we subsequently found that this tag was not necessary for binding. Presumably, in the absence of purified scWASP on the supported lipid bilayers the critical scWASP concentration required for actin network nucleation is not attained (4).

Reconstitution of Endocytic Actin Networks on Lipid Bilayers in Yeast Extract. scWASP-coated bilayers were incubated in freshly generated cytoplasmic extract and were then imaged. As previously observed with microbeads lacking a membrane bilayer, scWASP-coated supported lipid bilayers accumulated dense actin networks and associated actin-binding proteins (Fig. 1D). Membrane-associated filamentous actin was detected using GFP-tagged Sac6 (yeast fimbrin, an actin-binding protein, Fig. 1D) and fluorescent phalloidin, a small molecule that binds to filamentous actin (*SI Appendix*, Fig. S1B). Approximately 30% of beads broke symmetry and became motile, forming an actin tail behind the lipid-coated bead. Tail length was variable from bead to bead and between replicates and is likely related to the timing of stochastic symmetry breaking events. 3D reconstructions show tube-like actin structures trailing lipid-coated motile beads, with little Sac6 signal inside the tube (Movie S1). These structures resemble those previously observed in bacterial motility reconstitution in extracts (11). The actin networks associated with nonmotile beads failed to break symmetry but continued to assemble actin over time (Movie S2). Actin assembly on bilayers was dependent on the presence of scWASP (Fig. 1D). Addition of the actin monomer sequestering drug latrunculin A (LatA) to reactions prohibited actin tail assembly and bead motility.

Previous work demonstrated roles for anionic lipid species in CME site initiation and invagination, including phosphatidylserine
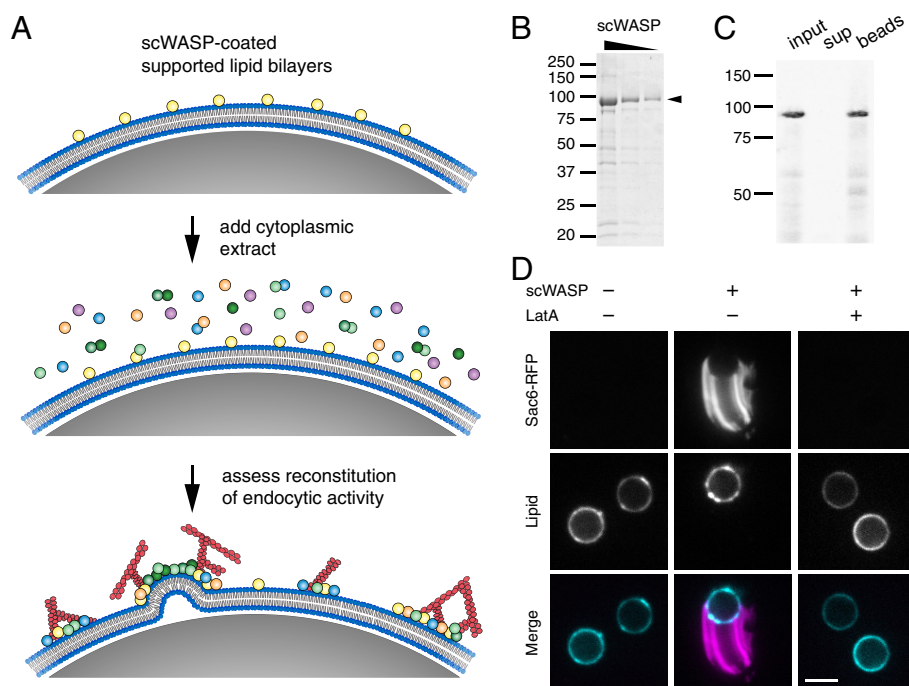
Fig. 1. Reconstitution of endocytic actin networks on supported lipid bilayers. (*A*) Schematic representation of the in vitro reconstitution assay. Purified scWASP (Las17) is attached to supported lipid bilayers, which are then incubated in yeast cytoplasmic extract, resulting in the assembly of endocytic actin networks. (*B*) GelCode-stained SDS-PAGE gel of purified scWASP (arrowhead). (*C*) Purified scWASP binds to supported lipid bilayers, as shown by western blot probed with an anti-Las17 antibody. (*D*) Sac6-RFP from yeast cytoplasmic extract labels actin networks assembled on scWASP-coated supported lipid bilayers (Atto647-DOPE, lipid). 180 μM latrunculin A (LatA) inhibits actin assembly on bilayers (Scale bar, 5 μm.).

(PS) and phosphatidylinositol 4,5 bisphosphate (PI(4,5)P$_2$) (22). Varying the lipid composition to include PS and/or PI(4,5)P$_2$ at concentrations used in previous bilayer reconstitution systems (17, 23–25) did not result in a pronounced effect on actin assembly on the beads, as measured by quantifying the percentage of beads that accumulated a Sac6 signal (*SI Appendix*, Fig. S1 *C* and *D*).

scWASP-Coated Bilayers Assemble the Machinery That Carries Out CME Internalization. To assess how faithfully the reconstitution system recapitulated in vivo CME events, we determined whether proteins downstream of scWASP in the endocytic pathway were recruited to the bilayers (Fig. 2*A*). We used extracts from yeast strains expressing a GFP-tagged protein of interest and Sac6-RFP to allow endocytic proteins to be located relative to the actin network.

Myo3 and Myo5 are type I myosins that facilitate endocytic actin assembly through their motor and NPF (nucleation-promoting factor) activities (26–28). They are required for endocytic vesicle internalization (21, 26, 29, 30). Myo5-GFP was localized primarily to the bilayers in areas of actin assembly, with trace amounts of Myo5-GFP also localizing to actin tails (Fig. 2*B*). These data are consistent with previous results on scWASP-coated microbeads (19) and with previous data showing that type I myosin does not leave the cell surface during vesicle internalization (31). Bzz1 was also recruited to bilayers in an scWASP-dependent manner (Fig. 2*B* and *SI Appendix*, Fig. S2*A*). Bzz1 is an scWASP-binding protein that relieves scWASP inhibition to promote actin assembly initiation (21, 32). On lipid bilayers with actin tails, Bzz1-GFP localized to the hemisphere of the lipid bilayer from which the actin tail protrudes. In contrast, Vrp1 [Wasp Interacting Protein (WIP)], which interacts directly with scWASP and Myo3/5 (21), was not observed or was only weakly observed on bilayers or associated with actin tails. Similarly, Bbc1 was not recruited to bilayers
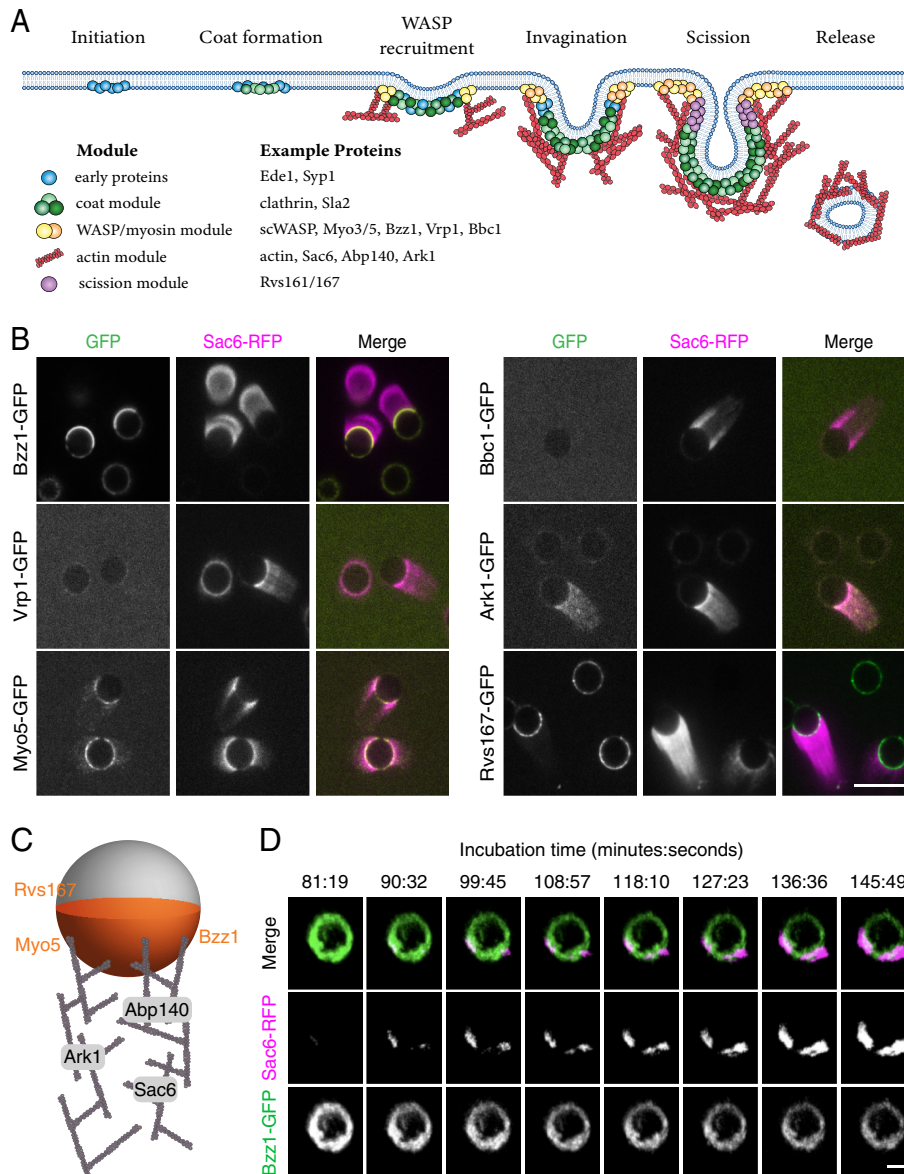

Fig. 2. scWASP-coated bilayers sequentially recruit downstream endocytic proteins. (*A*) Schematic representation of CME in *S. cerevisiae*. The schematic depiction is not drawn to scale. (*B*) Protein localization on scWASP-coated supported bilayers. Extracts were prepared from strains expressing Sac6-RFP and the indicated endocytic proteins tagged with GFP. Representative fluorescence images from three independent experiments are shown. (Scale bar, 10 μm.) (*C*) Localization of endocytic proteins on supported lipid bilayers and associated actin networks is represented in cartoon view. Bzz1, Rvs167, and Myo5 were observed primarily on lipid bilayers in the region of actin assembly. Ark1, Sac6, and Abp140 were associated with the actin network. (*D*) scWASP-coated beads were incubated in cytoplasmic extract from strains expressing Bzz1-GFP and Sac6-RFP. Representative montage of 3D rendered images from time-lapse confocal microscopy. Indicated time points (minutes:seconds) are relative to the moment cytoplasmic extract was added to beads (Scale bar, 2 μm.).

or actin tails under these conditions. Bbc1 is known to inhibit scWASP in later stages of endocytosis and to thereby control the speed and extent of inward vesicle movement (21, 30). Bbc1 absence from actin tails might reflect incomplete reconstitution of regulatory components. Following scWASP activation, there is a burst of actin assembly and recruitment of actin-associated proteins. As observed for Sac6-GFP, actin-binding protein Abp140-GFP was recruited to actin tails (*SI Appendix*, Fig. S2*B*). Additionally, the endocytic regulatory serine/threonine protein kinase Ark1 was observed in actin tails protruding from scWASP-coated lipid bilayers (Fig. 2*B*).

Further downstream of scWASP, heterodimeric N-BAR proteins Rvs161 and Rvs167 (yeast homologues of amphiphysin) contribute to vesicle scission and have been shown to tubulate membranes in vitro (30, 33). Observations in electron micrographs show that Rvs161/Rvs167 is concentrated at the bud neck of deeply invaginated clathrin-coated pits (34, 35). In our assay, Rvs167-GFP was recruited to scWASP-coated bilayers and was concentrated in the area of actin network formation, where it formed punctae (Fig. 2*B*).

We also analyzed whether proteins upstream of scWASP are recruited to the membranes. Sla2 links coat proteins to the actin cytoskeleton in vivo. However, it was not visible on scWASP-coated bilayers (*SI Appendix*, Fig. S2*C*).

These data are summarized in a cartoon schematic showing where each endocytic protein localizes on the scWASP-coated lipid bilayers (Fig. 2*C*). Our results are like those obtained previously with nonlipid-coated beads (19). The recruitment of multiple actin-binding proteins, nucleation-promoting factors, and actin regulatory components to the bilayers or actin tails, or both, indicates that our reconstituted system recapitulates self-assembly of the endocytic actin network. Furthermore, Rvs167 presence indicates recruitment of at least some of the machinery required to induce vesicle scission.

Protein Recruitment Order In Vitro Recapitulates CME Temporal Dynamics In Vivo.

As a test of whether the correct CME protein recruitment order is encoded in the proteins themselves, we assessed whether this sequence is recapitulated in the reconstituted system. The in vivo recruitment of proteins to endocytic sites follows a regular order that is highly conserved across species (1, 3, 36, 37) (Fig. 2*A*). To determine whether CME proteins accumulate on lipid bilayers in the correct physiological sequence, we observed reconstituted endocytic protein complexes as they formed in a flow chamber overtime. Fig. 2*D* shows time-lapse data from scWASP-coated beads after addition of cytoplasmic extract prepared from cells expressing Bzz1-GFP and Sac6-RFP. In cells, Bzz1 is present at the endocytic site immediately prior to the start of actin assembly (21, 32). Our in vitro data recapitulate this sequence with Bzz1 appearing on beads before Sac6 (Fig. 2*D* and Movie S2). Additionally, Bzz1 recruitment is scWASP-dependent (*SI Appendix*, Fig. S2*A*), indicating that the established sequence from scWASP to the regulatory factor (Bzz1) to actin assembly is preserved. Interestingly, Bzz1 localization on the bead is polarized prior to actin assembly, which then initiates from areas of high Bzz1 density.

These data demonstrate successful recapitulation of sequential endocytic protein assembly and establish that spatiotemporal recruitment is an intrinsic property of at least some endocytic proteins. It should be noted that while the recruitment order is preserved in vitro, the kinetics of recruitment do not replicate in vivo kinetics. In live cells, Bzz1 and Sac6 have lifetimes of approximately 15 to 17 and 11 to 15 s at the endocytic site, respectively (3, 21, 30). On supported lipid bilayers, Bzz1 is recruited to bilayers within seconds of extract addition, but there is a delay of up to 90 min prior to Sac6 arrival. The variance in length of time between recruitment events in the cytosolic extract versus the native yeast cytosolic environment could

reflect differences in the protein concentrations and energy conditions, or differences between length scales for in vivo endocytic events, which are on the nanometer scale, versus in vitro length scales for actin tails on the order of microns.

Vesicles Are Released from Sites of Endocytic Actin Network Assembly.

The supported lipid bilayer system described above reconstitutes actin-generated pushing forces on the micron scale, as demonstrated by bead motility. We next set out to determine whether these components could also drive nano-scale vesicle formation. In experiments similar to those described above to test for sequential CME protein recruitment, we next used a small amount of Atto647-DOPE as a marker of the lipid bilayer. The micrographs revealed tubules and smaller lipid protuberances in regions where endocytic proteins and actin assembled on the bilayers (*SI Appendix*, Fig. S3 *A* and *B*). In addition to tubulation, we often observed in static confocal micrographs small (diffraction-limited) lipid structures embedded in, or in the vicinity of, actin tails (Movies S3 and S4), which we hypothesized to be vesicles released from the supported-lipid bilayer. To determine whether these putative vesicles form by being pinched off from supported lipid bilayers, real-time imaging was performed. First, we systematically tested the effect of PS and PI(4,5)P$_2$ in lipid bilayers on vesicle accumulation in our assay. Addition of 5% PI(4,5)P$_2$ to our standard lipid mixture produced the highest frequency of actin-associated vesicles (*SI Appendix*, Table S2). In 37 time-lapse videos collected from four independent experiments, we observed spherical lipid structures breaking free from the lipid bilayer concurrent with a burst of actin polymerization at the same site (Fig. 3*A* and *SI Appendix*, Fig. S4*A*). The number of vesicles observed per bead (0.248 ± 0.291) was reduced dramatically by removing either scWASP (0.0476 ± 0.0638) or by treating reactions with LatA (0.0481 ± 0.0638); no vesicles were observed in the absence of cytoplasmic extract (*SI Appendix*, Table S3). To quantitatively analyze the dynamics of these vesiculation events and compare them to in vivo CME, we tracked vesicle formation and movement in 3D and measured fluorescence intensities and displacement over time (Fig. 3*B* and *SI Appendix*, Fig. S4*B*). Each vesicle track was temporally aligned at the displacement inflection point calculated using previously described techniques (*SI Appendix*, Fig. S5 and ref. 38). This alignment revealed a highly reproducible burst of actin assembly beginning approximately 15 min before the vesicle buds off from the bead (Fig. 3*C*). Bzz1 stays at the plasma membrane and is not observed to associate with the departing vesicle, consistent with previous data showing Bzz1's role in vesicle scission at the invagination base (21, 34, 39). The actin network continues to grow and propel the vesicle from the bead about 2 μm on average over about 10 min (Fig. 3*C*). This time scale is significantly longer than is seen in yeast, where the time from onset of actin assembly to vesicle scission is approximately 10 s. It is possible that ultracentrifugation and dilution of the cytoplasmic extract alter its composition sufficiently to affect reaction kinetics, or that the coupling between the membrane and actin is weak in the absence of Sla2. Alternatively, the assay may be reconstituting friction-mediated scission (40) in a system with less friction than in the native plasma membrane. Despite the difference in time scale, the sequence from scWASP to Bzz1 recruitment to actin assembly (as visualized by Sac6) to membrane pulling follows the order observed for endocytic events in vivo.

Given that endocytic events typically occur on a length scale that is below the diffraction limit of our fluorescence microscopy system, we employed correlative light and electron microscopy (CLEM) to achieve the necessary resolution to directly observe deformed membranes and free vesicles. We used beads 2 μm in
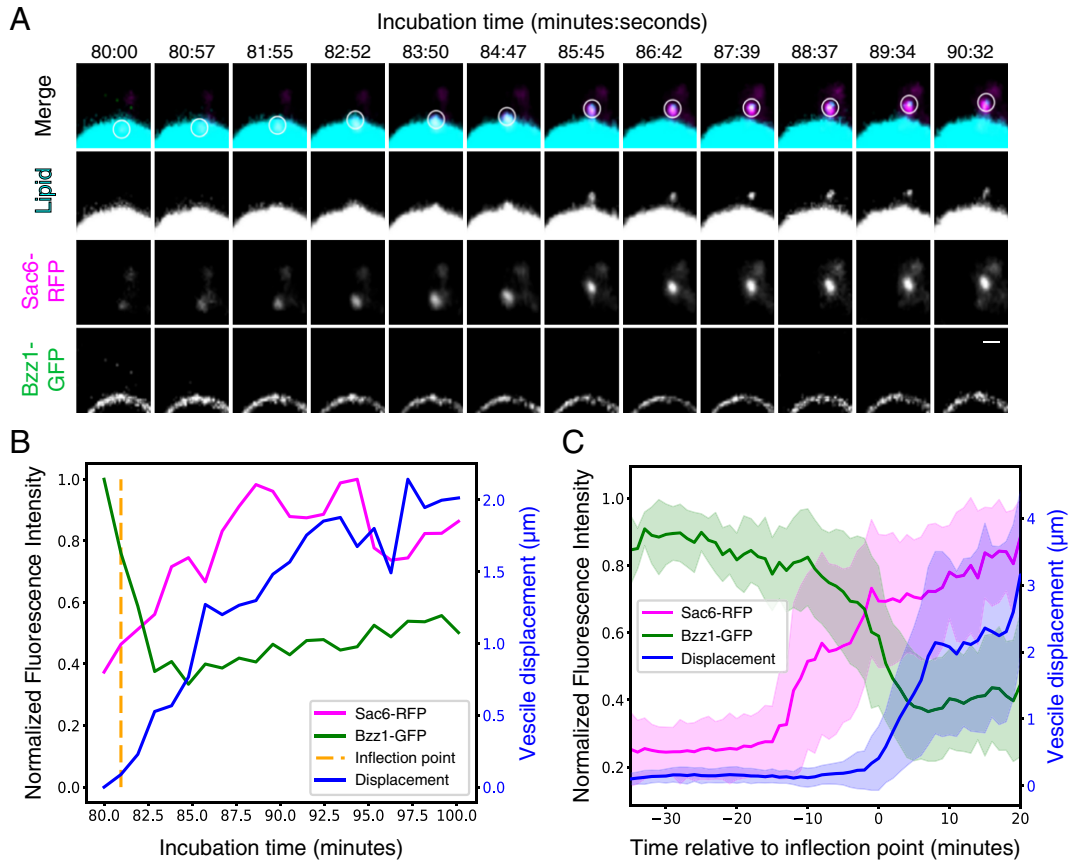
Fig. 3. Reconstitution of actin-mediated vesicle budding. Supported lipid bilayers were coated with scWASP and incubated in Bzz1-GFP Sac6-RFP cytoplasmic extracts for the indicated times. (*A*) Montage of a single vesiculation event. A maximum intensity projection 2 μm in depth is displayed for all channels. Bilayers include 2% Atto647-DOPE (cyan) to allow visualization of lipid. The white circle in the merged channel row indicates the region used for quantitative analysis. (Scale bar, 1 μm.) (*B*) Quantification trace of fluorescence intensities inside the white circle and vesicle displacement from the vesiculation event visualized in (*A*). The algorithmically determined inflection point is indicated by the vertical dotted line. (*C*) Mean fluorescence intensities and vesicle displacement with SD from all measured vesiculation events (n = 37). All traces were aligned in time by their respective inflection points prior to taking the mean and SD.

diameter (versus 5 μm in previous experiments) to improve the beads' spatial stability during sample processing for CLEM. Vesiculation events occurred on both size beads at similar rates (*SI Appendix,* Fig. S4 and Movies S6–S8). Transmission electron micrographs of lipid bilayers on beads in yeast extract revealed formation of scWASP-dependent membrane structures on the length scale of biological endocytic events (~50 to 100 nm, Fig. 4*A* and *SI Appendix,* Fig. S6*A–B*). A variety of membrane profiles were observed, including apparent tubules contiguous with the bead surface and vesicles some distance away from the bead (Fig. 4*A* and *SI Appendix,* Fig. S6). Corresponding light micrograph images demonstrated actin assembly around the beads (Fig. 4*A*, Sac6-GFP signal). To assess whether membrane deformation requires actin assembly, we sampled bilayers treated with LatA and observed a pronounced reduction in free vesicles, but an increase in small tubules and deformations at the membrane surface (Fig. 4*B*). Fewer free vesicles and membrane deformations were observed in samples lacking scWASP (Fig. 4*C*) and these features were entirely absent in samples lacking cytoplasmic extract (Fig. 4*D*). We lack 3D information in these TEM micrographs to allow us to determine whether the membrane structures are contiguous with the supported lipid bilayer. However, we have observed that vesicles move away from the beads in time-lapse imaging. Therefore, as a proxy for whether they are contiguous with the membrane or are distinct structures, we classified vesicles observed in EM by their distance from the bead surface (Fig. 4*E* and *SI Appendix,* Table S4). We observed an approximately 15-fold increase in the frequency of membrane structures

between 100 and 1,000 nm from the surface of scWASP-coated beads compared to the surface of beads lacking scWASP. Membranes observed in this region are likely vesicles derived from the supported lipid bilayer on the bead surface. Similar to our quantification of the time-lapse imaging data (*SI Appendix,* Table S3), more budding events were observed in reactions containing scWASP and extract in the absence of LatA. Of note, scWASP-containing beads treated with LatA to inhibit actin polymerization showed the highest frequency of membrane structures within 100 nm of the bead surface. These structures are likely invaginations of the bead supported lipid bilayer. Interestingly, the curvature-generating protein Bzz1 is recruited to supported lipid bilayers in a scWASP-dependent manner, independent of LatA treatment (*SI Appendix,* Fig. S6*C*). These data are consistent with a role for curvature generating proteins in early stages of membrane invagination and a known role for actin in driving membrane internalization and scission in yeast.

Conclusion

This work demonstrates that endocytic proteins and the actin network intrinsically embody the information sufficient to self-organize into a force-producing system capable of deforming a lipid bilayer and producing a vesicle. This work builds off other in vitro models for actin force generation, including those for *Listeria* motility (10), filopodia formation (41, 42) and actin-induced membrane phase separation (43). However, unlike previously reported systems, here actin is generating a pulling, not pushing, force. Moreover, time-lapse imaging revealed that the order of
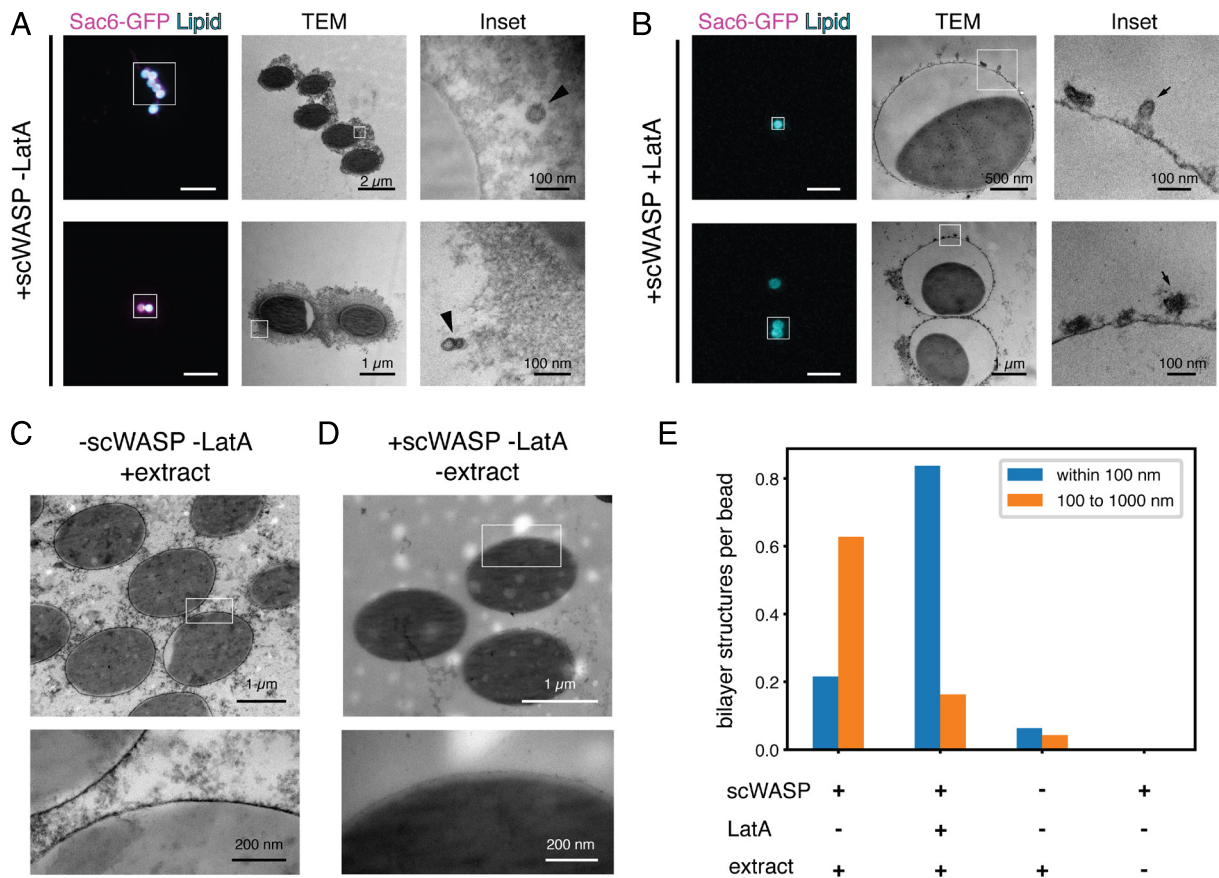
Fig. 4. Self-assembled endocytic actin networks deform lipid bilayers. (*A* and *B*) Representative CLEM images of scWASP-coated supported lipid bilayers incubated in extracts containing Sac6-GFP in the (*A*) presence or (*B*) absence of LatA. Bilayers include 2% Atto647-DOPE (cyan) to allow visualization of lipid. *Left* subpanels show light microscopy (Scale bar, 10 μm.). *Middle* and *Right* subpanels show transmission EM images of the regions indicated by white boxes. (*C* and *D*) Representative electron micrographs of supported bilayer reactions in the absence of (*C*) scWASP or (*D*) cytoplasmic extract. (*E*) Manual scoring of lipid bilayer tubules and vesicles in EM sections prepared from the indicated reaction conditions.

molecular events was faithfully reconstituted, and electron microscopy showed that these membrane remodeling events are on the size scale observed in yeast endocytosis.

Interestingly, vesicle generation in our reconstituted system occurs in the absence of certain upstream structural and regulatory factors including Sla2 and Bbc1. It is possible that other coat proteins that we did not attempt to localize in this study are recruited to the in vitro system. Our data are consistent with previous findings, which showed that many coat proteins and initiation factors are not necessary for endocytic vesicle formation. Endocytosis still occurs in clathrin null mutants, although the number of endocytic sites is reduced (30, 44–46). A previous study examined CME in yeast with null alleles of genes encoding seven initiation factors and coat proteins and determined that membrane bending and vesicle budding were largely unperturbed (8). These observations are consistent with the existence of multiple endocytic pathways in various cell types that require actin but do not require clathrin or its associated coat proteins (47, 48). In light of these observations, we propose that a network of actin and associated proteins might constitute a primitive endocytic machinery that diversified through evolution to give rise to multiple vesicle-forming processes, with coat proteins and other accessory factors added later as evolutionary embellishments.

In the future, addition of cargo and proteins upstream of scWASP in the CME pathway to this in vitro reconstitution assay promises to provide valuable mechanistic insights into the roles of cargo, coat proteins, and other regulatory factors. We anticipate

that coat proteins would be required to reconstitute selective cargo recruitment, as shown previously in yeast (8). Additionally, the in vitro assay provides a system in which effects of differing lipid composition on CME can be analyzed without off-target effects that confound such studies in live cells.

This work establishes that vesicle pulling, and scission, are intrinsic to the ensemble activities of the endocytic actin network. Future work using this assay will allow us to elucidate the roles of individual proteins and lipid species in vesicle generation.

Materials and Methods

Protein Purification. Yeast WASP (Las17) was cloned into the p363 overexpression plasmid using PacI and XmaI restriction sites to be in frame with a C-terminal TEV site, 3× StreptagII, and 9× His tag. The recombinant protein was overexpressed in yeast using a GAL induction system in the D1074 strain and purified as described previously (50). Briefly, protein expression was induced with 2% galactose for 6 to 8 h at 30 °C. Following induction, cells were flash frozen. Frozen cells were lysed by mechanical shearing in a cryogenic grinder (SPEX SamplePrep). The resulting powder was reconstituted in buffer containing protease inhibitors (Roche) and centrifuged at 80k rpm for 20 min at 4 °C. The supernatant was passed through a 0.45-μm syringe filter and then applied to a HisTrap column. Samples containing Las17 were pooled and dialyzed in a Slide-a-Lyzer cassette (Thermo Fisher) after addition of TEV protease. After a brief

incubation with Ni-agarose to remove the protease and cleaved His tag, Las17 was concentrated in an Ultra-4 centrifugal filter device (Amicon). Aliquots of purified Las17 were flash frozen in liquid nitrogen.

Supported Lipid Bilayer Production. Supported lipid bilayers were prepared using a previously published protocol with minor modifications (51). Briefly, chloroform stocks of lipids (Avanti Polar Lipids) were combined in a glass vial etched with Piranha solution (3:1 H_2SO_4/H_2O_2) according to the molar ratios listed for each experiment. Unless otherwise listed, the lipid composition used for each experiment was 75% phosphatidylcholine (PC), 5% DGS-NTA, 20% phosphatidylserine (PS). In instances where a membrane dye was added to visualize membranes, PC concentration was lowered accordingly. The lipid mixture was dried at 42 °C under vacuum using a rotary evaporator. After brief exposure to nitrogen, the dried lipid film was rehydrated in deionized water to 1 mg/mL. The mixture was passed through a microextruder (Avanti Polar Lipids) fitted with a 0.1-μm filter 11 times to generate small unilamellar vesicles (SUVs). SUVs were used immediately or stored for up to 5 d at 4 °C.

Polystyrene or silica microspheres (Bangs Laboratories) were cleaned for 15 min in 1% Helmenex, followed by three wash steps in ddH$_2$O. SUVs diluted 1:5 in 10× TBS (to a final concentration of 2× TBS) were incubated with the microbeads, generating supported lipid bilayers through self-assembly. Unruptured vesicles were removed via multiple wash steps in TBS.

Generation of Whole-Cell Lysates. Cells were grown in YPD at 25 °C to an OD$_{600}$ of 0.6 to 0.8, as measured on an Ultrospec 10 Cell Density Meter (Amersham). Cells from 4 L of culture were harvested by centrifugation, washed in cold water, and centrifuged again. Standing moisture was removed from pellets, and cells were flash frozen in liquid N$_2$ and then stored at −80 °C. Frozen cultures were lysed by mechanical shearing in a prechilled cryogenic grinder (SPEX SamplePrep) using a medium-sized SPEX vial that had been prechilled in liquid nitrogen. Milling consisted of a 5 min prechill followed by 6 to 10 cycles comprising 3 min of grinding and 1 min of rest. The sample vial remained submerged in liquid N$_2$ throughout the milling process. Powdered lysate was collected in a 50-mL conical vial that had been prechilled in liquid nitrogen. Lysate preparations stored at −80 °C were stable for >6 mo but were highly sensitive to temperature excursions.

Yeast Extract Preparation. HK buffer (40 mM HEPES, pH 7.5, 200 mM KCl, and 1 mM PMSF) was supplemented with cOmplete mini EDTA-free protease inhibitor cocktail (Roche), according to manufacturer specifications. Powdered lysate was weighed out into a prechilled 5-mL glass beaker using a prechilled spatula. Then, 875 μL of supplemented HK buffer at 4 °C was added to each gram of yeast powder. After thawing on ice, samples were centrifuged in a prechilled polycarbonate ultracentrifuge tube for 25 min at 345,000 × g at 4 °C. The cleared supernatant was collected immediately following the centrifuge run using a syringe to transfer it to a prechilled 1.5-mL tube and was then used in an assay within 10 min of the final ultracentrifugation step. Care was taken to avoid disturbing either the pellet or the white lipid layer. Reconstitution of actin assembly was impaired by gaps exceeding 10 min between the end of centrifugation and addition to bilayers, as well as by any warming of the powdered lysate above−80 °C prior to thawing in the supplemented HK buffer.

Membrane Functionalization and Bead Assay. For 1 h, 180 nM yeast WASP (Las17) was incubated on the membranes. Beads were washed and then incubated in 1% casein for 15 min to block nonspecific binding. After washing to remove excess casein, beads were stored in 1× TBS for up to 1 h. Then, 1 to 2 μL functionalized bilayers were added to the cytosolic extract to a total reaction volume of 20 μL. In addition, 1 mM ATP and, where noted, 180 μM LatA (Sigma Aldrich) were added immediately to the bilayer and extract mixture. Microbeads were spotted on slides and imaged within 1 h.

Microscopy and Image Analysis.
Fluorescence microscopy. Except where noted otherwise, all images were acquired on a Nikon Eclipse Ti inverted Yokogawa spinning disk confocal microscope fitted with Andor CSU-X spinning disc confocal equipment and controlled by Nikon Elements software. Imaging was performed using a 100× 1.45 NA Plan Apo λ oil immersion objective and an Andor IXon X3 EM-CCD camera. GFP, RFP, and Atto647 fluorescence were excited using 488-, 561- and 638-nm lasers, respectively. Images for figure panel S1C were collected using a Nikon Eclipse

Ti microscope equipped with a 100× 1.4 NA Plan Apo VC oil objective and an Andor Neo sCMOS camera. The system was controlled using Metamorph software (Molecular Devices). Images for figure panels 4A (lower subpanel) and 4B (both subpanels) were acquired on a AxioObserver Zeiss LSM 710 Laser Scanning Confocal with 40× 1.4 NA Plan Apo oil immersion objective and PMT detector. GFP and Atto647 fluorescence was excited using 488- and 633-nm lasers, respectively. The system was controlled with Zen 2010 software. All imaging devices were kept in rooms maintained at 23 to 25 °C.

Fluorescence recovery after photobleaching. Membrane fluidity was assessed using fluorescence recovery after photobleaching (FRAP) performed on a Zeiss LSM 710 confocal microscope fitted with a Plan-Apochromat 63× 1.40 NA oil immersion DIC M27 and Zen software. An ROI drawn over a portion of the bilayer was bleached using 594-nm laser light at 100% laser power for 50 iterations. Images were taken every 780 ms before and after bleaching. Images were analyzed using ImageJ software. The plot profile function in Fiji was used to measure the signal intensity of TexasRed-DHPE in the bleached ROI and the opposite (unbleached) side of the bilayer. FRAP data were normalized to the highest and lowest mean values in the prebleach condition.

CLEM. Supported lipid bilayers were generated on polystyrene microbeads and incubated with 500 nM scWASP and cytosolic extract, as described above. Reactions were fixed in 4% paraformaldehyde, 0.05% glutaraldehyde for at least 30 min at 4 °C. Beads were deposited on poly-L-lysine-coated 35-mm gridded glass-bottom dishes (MatTek). After washing, adherent beads were embedded in 2% low melting point agarose (Electron Microscopy Sciences) and submerged in 1× TBS for microscopy. Regions of interest were identified by Atto647-DOPE and Sac6-GFP fluorescence signal, and then mapped to spatial coordinates on the gridded coverslip by brightfield imaging. Samples were then washed in 1× PBS and stained with 1% osmium tetroxide and 1.6% potassium ferricyanide at 4 °C for 45 min. Following additional washes with PBS, and a quick exchange in water, samples were dehydrated with an ascending gradient of ethanol followed by pure ethanol before they were progressively infiltrated with resin and left overnight in unaccelerated Epon resin (Ted Pella). Epon resin with accelerant was exchanged onto the sample three times, then the dishes were incubated at 60 °C for 16 to 20 h for resin polymerization. Following polymerization, the glass coverslips were removed using ultra-thin Personna razor blades (EMS). CLEM was performed to visualize specific beads within regions of interest. Regions of interest, identified by the gridded alpha-numerical labeling on the plates were carefully removed, precisely trimmed to the area of interest, and mounted on a blank resin block with cyanoacrylate glue for sectioning. Serial thin sections (80 nm) were cut using a Leica UC6 ultramicrotome (Leica) from the surface of the block until approximately 4 to 5 microns in to ensure complete capture of the bead. Section-ribbons were then collected sequentially onto formvar-coated slots or 50 mesh grids. The grids were poststained with 2% uranyl acetate followed by Reynold's lead citrate, for 5 min each. The sections were imaged using a FEI Tecnai 12 120kV TEM (FEI) and data recorded using either a Gatan US1000 CCD with Digital Micrograph 3 or a Gatan Rio 16 CMOS with Gatan Microscopy Suite software (Gatan Inc.). Images were adjusted for brightness and contrast in ImageJ (NIH), and rotated, but otherwise unaltered.

Image analysis. Images were processed using ImageJ software. Pixel intensity values were rescaled identically for all images from an experiment. To allow visualization of small structures, some pixels in some images were intentionally saturated. To quantify Sac6 accumulation on lipid bilayers of varying compositions, beads were manually counted in the DIC channel and then scored for presence or absence of Sac6 fluorescence.

Additional image processing of time-lapse spinning disc confocal fluorescence microscopy data was performed using ImageJ plugins following recommendations by Picco et al. (52). First, background subtraction was applied to raw data from each channel using a rolling ball algorithm with 100 pixel radius. We then performed bleach correction with an exponential decay model on each individual channel except when imaging Sac6-RFP, because for this marker there was no decay in fluorescence signal over the course of our time-lapses. Individual beads were then cropped and processed with a 3D drift correction algorithm so that positions of vesicles could later be measured relative to their source bead. The resulting multichannel volumetric time-lapse processed data were then rendered in 3D and assembled into montages using custom python scripts [available on GitHub (https://github.com/DrubinBarnes/Stoops_Ferrin_et_al_2023)].

To quantify vesiculation dynamics, we used the TrackMate plugin of ImageJ to manually track the position of vesicles in time-lapse data after the processing steps

described in the previous paragraph. We measured the 3D displacement of each tracked vesicle from its starting position overtime, as well as the average fluorescence intensity of a 0.4-μm radius sphere around the center of each vesicle over time. To collectively analyze data for all tracked vesicles, we first aligned each individual trajectory in time by the inflection point of the displacement curve (adapted from ref. 38). The inflection point was defined as the time point at which the vesicle displacement was the maximum negative difference from a linear regression fit to each vesiculation event trace, out of all the time points before the point of the maximum positive difference. Aligned fluorescence intensity curves were normalized to the maximum value for each vesicle before calculating the average and SD for all tracked vesicles.

Data, Materials, and Software Availability. All study data are included in the article and/or supporting information.

Author affiliations: [a]Department of Molecular and Cell Biology, University of California, Berkeley, CA 94720; and [b]Electron Microscope Laboratory, University of California, Berkeley, CA 94720

1. M. Kaksonen, Y. Sun, D. G. Drubin, A pathway for association of receptors, adaptors, and actin during endocytic internalization. *Cell* **115**, 475–487 (2003).
2. C. J. Merrifield, M. Kaksonen, Endocytic accessory factors and regulation of clathrin-mediated endocytosis. *Cold Spring Harb. Perspect. Biol.* **6**, a016733 (2014).
3. R. T. A. Pedersen, J. E. Hassinger, P. Marchando, D. G. Drubin, Spatial regulation of clathrin-mediated endocytosis through position-dependent site maturation. *J. Cell Biol.* **219**, 934 (2020).
4. Y. Sun et al., Switch-like Arp2/3 activation upon WASP and WIP recruitment to an apparent threshold level by multivalent linker proteins in vivo. *Elife* **6**, e29140 (2017).
5. S. Aghamohammadzadeh, K. R. Ayscough, Differential requirements for actin during yeast and mammalian endocytosis. *Nat. Cell Biol.* **11**, 1039–1042 (2009).
6. E. B. Lewellyn et al., An engineered minimal WASP-myosin fusion protein reveals essential functions for endocytosis. *Dev. Cell* **35**, 281–294 (2015).
7. M. Bhave et al., Functional characterization of 67 endocytic accessory proteins using multiparametric quantitative analysis of CCP dynamics. *Proc. Natl. Acad. Sci. U.S.A.* **117**, 31591–31602 (2020).
8. T. Brach, C. Godlee, I. Moeller-Hansen, D. Boeke, M. Kaksonen, The initiation of clathrin-mediated endocytosis is mechanistically highly flexible. *Curr. Biol.* **24**, 548–554 (2014).
9. A. P. Liu, D. A. Fletcher, Biology under construction: In vitro reconstitution of cellular function. *Nat. Rev. Mol. Cell Biol.* **10**, 644–650 (2009).
10. T. P. Loisel, R. Boujemaa, D. Pantaloni, M. F. Carlier, Reconstitution of actin-based motility of Listeria and Shigella using pure proteins. *Nature* **401**, 613–616 (1999).
11. W. M. Brieher, M. Coughlin, T. J. Mitchison, Fascin-mediated propulsion of Listeria monocytogenes independent of frequent nucleation by the Arp2/3 complex. *J. Cell Biol.* **165**, 233–242 (2004).
12. O. Akin, R. D. Mullins, Capping protein increases the rate of actin-based motility by promoting filament nucleation by the Arp2/3 complex. *Cell* **133**, 841–851 (2008).
13. R. Heald, Self-organization of microtubules into bipolar spindles around artificial chromosomes in Xenopus egg extracts. *Nature* **401**, 420–425 (1996).
14. J. Gaetz, Z. Gueroui, A. Libchaber, T. M. Kapoor, Examining how the spatial organization of chromatin signals influences metaphase spindle assembly. *Nat. Cell Biol.* **8**, 924–932 (2006).
15. T. Weber et al., SNAREpins: Minimal machinery for membrane fusion. *Cell* **92**, 759–772 (1998).
16. A. Spang, R. Schekman, Reconstitution of retrograde transport from the Golgi to the ER in vitro. *J. Cell Biol.* **143**, 589–599 (1998).
17. T. J. Pucadyil, S. L. Schmid, Real-time visualization of dynamin-catalyzed membrane fission and vesicle release. *Cell* **135**, 1263–1275 (2008).
18. M. Wu et al., Coupling between clathrin-dependent endocytic budding and F-BAR-dependent tubulation in a cell-free system. *Nat. Cell Biol.* **12**, 902–908 (2010).
19. A. Michelot et al., Reconstitution and protein composition analysis of endocytic actin patches. *Curr. Biol.* **20**, 1890–1899 (2010).
20. A. A. Rodal, A. L. Manning, B. L. Goode, D. G. Drubin, Negative regulation of yeast WASp by two SH3 domain-containing proteins. *Curr. Biol.* **13**, 1000–1008 (2003).
21. Y. Sun, A. C. Martin, D. G. Drubin, Endocytic internalization in budding yeast requires coordinated actin nucleation and myosin motor activity. *Dev. Cell* **11**, 33–46 (2006).
22. Y. Sun, D. G. Drubin, The functions of anionic phospholipids during clathrin-mediated endocytosis site initiation and vesicle formation. *J. Cell Sci.* **125**, 6157–6165 (2012).
23. H. Zhao et al., Membrane-sculpting BAR domains generate stable lipid microdomains. *Cell Rep.* **4**, 1213–1223 (2013).
24. C. F. E. Schroer et al., Charge-dependent interactions of monomeric and filamentous actin with lipid bilayers. *Proc. Natl. Acad. Sci. U.S.A.* **117**, 5861–5872 (2020).
25. K. J. Day et al., Liquid-like protein interactions catalyze assembly of endocytic vesicles. *Nat. Cell Biol.* **23**, 366–376 (2021).
26. M. I. Geli, H. Riezman, Role of type I myosins in receptor-mediated endocytosis in yeast. *Science* **272**, 533–535 (1996).
27. H. E. Manenschijn et al., Type-I myosins promote actin polymerization to drive membrane bending in endocytosis. *Elife* **8**, e44215 (2019).
28. R. T. A. Pedersen, D. G. Drubin, Type I myosins anchor actin assembly to the plasma membrane during clathrin-mediated endocytosis. *J. Cell Biol.* **218**, 1138–1147 (2019).
29. H. V. Goodson, B. L. Anderson, H. M. Warrick, L. A. Pon, J. A. Spudich, Synthetic lethality screen identifies a novel yeast myosin I gene (MYO5): Myosin I proteins are required for polarization of the actin cytoskeleton. *J. Cell Biol.* **133**, 1277–1291 (1996).
30. M. Kaksonen, C. P. Toret, D. G. Drubin, A modular design for the clathrin- and actin-mediated endocytosis machinery. *Cell* **123**, 305–320 (2005).
31. G. A. Jonsdottir, R. Li, Dynamics of yeast Myosin I: Evidence for a possible role in scission of endocytic vesicles. *Curr. Biol.* **14**, 1604–1609 (2004).
32. A. Soulard et al., Saccharomyces cerevisiae Bzz1p is implicated with type I myosins in actin patch polarization and is able to recruit actin-polymerizing machinery in vitro. *Mol. Cell. Biol.* **22**, 7889–7906 (2002).
33. J.-Y. Youn et al., Dissecting BAR domain function in the yeast Amphiphysins Rvs161 and Rvs167 during endocytosis. *Mol. Biol. Cell* **21**, 3054–3069 (2010).
34. F.-Z. Idrissi et al., Distinct acto/myosin-I structures associate with endocytic profiles at the plasma membrane. *J. Cell Biol.* **180**, 1219–1232 (2008).
35. A. Picco, M. Mund, J. Ries, F. Nédélec, M. Kaksonen, Visualizing the functional architecture of the endocytic machinery. *Elife* **4**, e04535 (2015).
36. M. Kaksonen, C. P. Toret, D. G. Drubin, Harnessing actin dynamics for clathrin-mediated endocytosis. *Nat. Rev. Mol. Cell Biol.* **7**, 404–414 (2006).
37. R. Lu, D. G. Drubin, Y. Sun, Clathrin-mediated endocytosis in budding yeast at a glance. *J. Cell. Sci.* **129**, 1531–1536 (2016).
38. Y. Sun et al., Direct comparison of clathrin-mediated endocytosis in budding and fission yeast reveals conserved and evolvable features. *Elife* **8**, e50749 (2019).
39. T. Kishimoto et al., Determinants of endocytic membrane geometry, stability, and scission. *Proc. Natl. Acad. Sci. U.S.A.* **108**, E979–E988 (2011).
40. M. Simunovic et al., Friction mediates scission of tubular membranes scaffolded by BAR proteins. *Cell* **170**, 172–184.e11 (2017).
41. A. P. Liu et al., Membrane-induced bundling of actin filaments. *Nat. Phys.* **4**, 789–793 (2008).
42. K. Lee, J. L. Gallop, K. Rambani, M. W. Kirschner, Self-assembly of filopodia-like structures on supported lipid bilayers. *Science* **329**, 1341–1345 (2010).
43. A. P. Liu, D. A. Fletcher, Actin polymerization serves as a membrane domain switch in model lipid bilayers. *Biophys. J.* **91**, 4064–4070 (2006).
44. G. S. Payne, R. Schekman, A test of clathrin function in protein secretion and cell growth. *Science* **230**, 1009–1014 (1985).
45. D. S. Chu, B. Pishvaee, G. S. Payne, The light chain subunit is required for clathrin function in Saccharomyces cerevisiae. *J. Biol. Chem.* **271**, 33123–33130 (1996).
46. T. M. Newpher, S. K. Lemmon, Clathrin is important for normal actin dynamics and progression of Sla2p-containing patches during endocytosis in yeast. *Traffic* **7**, 574–588 (2006).
47. S. Mayor, R. E. Pagano, Pathways of clathrin-independent endocytosis. *Nat. Rev. Mol. Cell Biol.* **8**, 603–612 (2007).
48. K. Sandvig, S. Kavaliauskiene, T. Skotland, Clathrin-independent endocytosis: An increasing degree of complexity. *Histochem Cell Biol.* **150**, 107–118 (2018).
49. M. S. Longtine et al., Additional modules for versatile and economical PCR-based gene deletion and modification in Saccharomyces cerevisiae. *Yeast* **14**, 953–961 (1998).
50. J. St-Pierre et al., Polo kinase regulates mitotic chromosome condensation by hyperactivation of condensin DNA supercoiling activity. *Mol. Cell* **34**, 416–426 (2009).
51. W. C. Lin, C. H. Yu, S. Triffo, J. T. Groves, Supported membrane formation, characterization, functionalization, and patterning for application in biological science and technology. *Curr. Protoc. Chem. Biol.* **2**, 235–269 (2010).
52. A. Picco, M. Kaksonen, Precise tracking of the dynamics of multiple proteins in endocytic events. *Methods Cell Biol.* **139**, 51–68 (2017).